Two-Dimensional Numerical Simulation of Bed-Load Transport of a Finite-Depth Sediment Layer: Applications to Channel Flushing

Daniel Caviedes-Voullième[1]; Mario Morales-Hernández[2]; Carmelo Juez[3]; Asier Lacasta[4]; and Pilar García-Navarro, Aff.M.ASCE[5]

Abstract: Numerical modeling of bed-load transport in shallow flows, particularly oriented toward environmental flows, is an active field of research. Nevertheless, other possible applications exist. In particular, bed-load transport phenomena are relevant in urban drainage systems, including sewers. However, few applications of coupled two-dimensional (2D) shallow-water and bed-load transport models can be found, and their transfer from environmental applications—usually river and floodplain—into sewer applications requires some adaptation. Unlike to river systems, where there is a thick layer of sediment that constitutes a movable riverbed, sewer systems have thin layers of sediment that need to be removed, thus exposing a rigid, nonerodible surface. This problem requires careful numerical treatment to avoid generating errors and instability in the simulation. This paper deals with a numerical approach to tackle this issue in an efficient way that allows large-scale studies to be performed and provides empirical evidence that the proposed approach is accurate and applicable for sewage and channel-flushing problems. **DOI: 10.1061/(ASCE)HY.1943-7900.0001337.**

Author keywords: Shallow water; Exner equation; Maximum erodability; Finite-depth sediment layer; Thin sediment layer; Partially erodible bed; Channel flushing; Graphics-processing unit (GPU) computing.

Introduction

Shallow flows and sediment transport have received wide attention from the modeling community. Accurate and efficient solvers to model unsteady sediment transport problems have been demanded strongly by researchers and practitioners in fields such as river engineering (Parker 1979; Wu 2004) and coastal engineering (Butt and Russel 2000; Masselink and Russel 2006; Bakhtyar et al. 2009). Many of these applications have been successfully addressed with two-dimensional (2D) shallow-water models coupled to bed-load and suspended-transport solvers (Begnudelli and Sanders 2006; Xia et al. 2010; Soares-Frazao and Zech 2011; Hou et al. 2015).

On the other hand, flushing of sedimented channels is a relevant topic in sewer design and sewer management (Ashley and Verbanck 1996; Staufer et al. 2007; Schaffner 2008; Schlütter 1999) and for hydraulic structures in general. Sewers are prone to sediment deposits that, because of the underground nature of sewer systems, are difficult, expensive, or even impossible to clean manually or mechanically. Furthermore, sedimentation in sewers results in a reduction in hydraulic efficiency in terms of both conveyance and storage and, in the case of sanitary sewers, even corrosion and gas emissions. Flushing is an obvious strategy to keep these systems operative. However, the nature of flushing events, which includes fast transients of coupled hydrodynamics and sediment dynamics, makes their understanding, modeling, and prediction very complex. Numerical simulation is a powerful tool to address this need (Dettmar 2007; Schlütter 1999; Staufer et al. 2007). Although numerical models have been applied and reported in this field of application (Campisano et al. 2004, 2013; Creaco and Bertrand-Krajewski 2009), it seems that this field has not yet widely benefited from the most recent advances in numerical models oriented toward more environmental flows such as in rivers and coasts, although it was recently pointed out (Shirazi et al. 2014) that there is a growing need for coupled and robust unsteady solvers.

Sediment transport in sewer systems has been addressed in different ways. For some flushing applications, three-dimensional (3D) Reynolds-averaged Navier-Stokes (RANS) models have been proposed (Schaffner 2008), but because of their enormous computational cost such models are unlikely to be a suitable tool for large-scale tests and sensitivity analysis. Arguably, RANS equations are unnecessary and shallow-water equations (SWEs) coupled with sediment transport equations suffice. In particular, this problem has been numerically addressed mainly with one-dimensional (1D) SWE models (Schaffner 2008; Campisano et al. 2004; Creaco and Bertrand-Krajewski 2009). The fundamental argument is of course that sewer systems are a network of 1D conduits. Nevertheless, when sewer conduits and collectors show significantly large

[1]Chair for Hydrology and Water Resource Management, Brandenburg Univ. of Technology, Siemens-Halske Ring, 03044 Cottbus, Germany; Computational Hydraulics Group, Laboratorio de Investigación en Fluidodinámica y Tecnologías de la Combustión, Consejo Superior de Investigaciones Científicas-Universidad Zaragoza, 50018 Zaragoza, Spain (corresponding author). ORCID: https://orcid.org/0000-0001-7871-7544. E-mail: caviedes@b-tu.de

[2]Computational Hydraulics Group, Laboratorio de Investigación en Fluidodinámica y Tecnologías de la Combustión, Consejo Superior de Investigaciones Científicas-Universidad Zaragoza, 50018 Zaragoza, Spain.

[3]École Polytechnique Fédérale de Lausanne, Laboratoire de Constructions Hydrauliques, Lausanne, Switzerland.

[4]Computational Hydraulics Group, Laboratorio de Investigación en Fluidodinámica y Tecnologías de la Combustión, Consejo Superior de Investigaciones Científicas-Universidad Zaragoza, 50018 Zaragoza, Spain.

[5]Professor, Computational Hydraulics Group, Laboratorio de Investigación en Fluidodinámica y Tecnologías de la Combustión, Consejo Superior de Investigaciones Científicas-Universidad Zaragoza, 50018 Zaragoza, Spain.

Note. This manuscript was submitted on June 16, 2016; approved on February 28, 2017; published online on June 19, 2017. Discussion period open until November 19, 2017; separate discussions must be submitted for individual papers. This paper is part of the ***Journal of Hydraulic Engineering***, © ASCE, ISSN 0733-9429.

geometrical dimensions, as compared with sediment layers, 2D models might also be appealing to better represent and predict sediment transport, which is very strongly determined by channel geometry and the (possibly 2D) velocity field.

One of the reasons that environmentally oriented models have not yet been adopted for sewer flushing is that most of them do not effectively address the issue of finite-depth sediment layers (alternatively referred to as partially nonerodible bottoms in the literature), which largely influence the dynamics (Ashley and Verbanck 1996; Struiksma 1999). Rivers and coasts typically have sediments of considerable height over a rigid rockbed. Therefore, for practical purposes there is little need to represent the underlying rockbed or to manage the mathematical issues that arise in sediment transport equations when the sediment is completely removed and the rockbed becomes exposed. Conversely, hydraulic structures, such as sewer pipes and tunnels, are very prone to this issue. In particular, the goal of sewer flushing is precisely to expose the rigid, nonerodible surface of the pipe or tunnel. It naturally follows that, to migrate numerical models developed in the context of environmental flows to these engineered systems, the issue of properly handling finite-depth sediment layers must be tackled. Very little research has been reported on this issue. Struiksma (1999) proposed a correction of transport capacity and acknowledged the need for time-step size reduction. Rulot et al. (2012) proposed an iterative flux correction approximating an optimization problem. Ortiz et al. (2015) proposed a flux correction in a finite-element context. Rosatti and Zugliani (2015) studied the issue in the finite-volume context by means of a composite Riemann problemin which not only states but also the system of equations change at the Riemann interface, although this requires a strong coupling of hydraulic and morphodynamic equations. Morales de Luna et al. (2010) made use of a modified Meyer–Peter-Müller expression to account for sediment thickness, thus ensuring that bed-load transport vanishes as depth approaches zero. Their approach, however depended on a typical average sediment height acting as a normalization parameter that may be difficult to define and was also reported to be computationally up to twice as expensive as solutions with standard Meyer–Peter-Müller solutions.

In addition, the underlying stochastic nature of precipitation and bed-load sediment transport, and the uncertainties, for example, in the type and quantities of sediment entering sewer systems (Ashley and Verbanck 1996), require that numerical models be computationally efficient so that sensitivity analyses—which require a large number of scenarios and simulations—are feasible. The strategy to ensure this is twofold: ensuring that the numerical scheme is efficient (i.e., that time-step reduction is avoided, thus reducing the overhead of dealing with finite-depth sediment layers) and ensuring that the implementation of the model is up to date with computational hardware, making the best use of parallelization strategies and general-purpose graphics-processing unit (GPU) computing (Juez et al. 2016; Lacasta et al. 2014).

In this work, a 2D shallow-water model coupled to bed-transport models originally proposed and validated for environment-oriented flows is extended to handle finite-depth sediment layers, with a particular focus on enabling the flushing of man-made hydraulic structures. Specifically, a simple yet effective strategy to deal with finite-depth sediment layers is proposed and tested. To complement this, the applicability of the proposed numerical model is assessed on academic and experimental benchmarks and in a full-scale sewer system project in Spain.

The paper is structured as follows. First, the mathematical model for shallow-water flow and bed-load transport is summarized and a review of the key elements of the underlying numerical scheme and the proposed technique to deal with finite-depth sediment layers is presented. Next, validation tests against experimental results are shown and a field-scale test of the applicability and usefulness of the model is discussed. Finally, key conclusions are presented.

Mathematical Model

Shallow-Water Equations

The shallow-water equations in two dimensions are as follows:

$$\frac{\partial \mathbf{U}}{\partial t} + \nabla \cdot \mathbf{F}(\mathbf{U}) = \mathbf{S}(\mathbf{U}) \tag{1}$$

where $\mathbf{U}(x, t)$ = vector of conserved variables; and

$$\mathbf{U} = [h, q_x, q_y]^\top \tag{2}$$

where h = water depth [L]; $q_x = hu$ = momentum [L^2/T] in the x-direction; $q_y = hv$ = momentum [L^2/T] in the y-direction; u and v = components of the velocity vector $\mathbf{u}$; and [L/T] = x- and y-directions.

The flux components $\mathbf{F}(\mathbf{U}) = [\mathbf{E}(\mathbf{U}), \mathbf{G}(\mathbf{U})]$ in Eq. (1) are

$$\mathbf{E}(\mathbf{U}) = \left[q_x, \frac{q_x^2}{h} + \frac{gh^2}{2}, \frac{q_x q_y}{h}\right]^\top$$
$$\mathbf{G}(\mathbf{U}) = \left[q_y, \frac{q_x q_y}{h}, \frac{q_y^2}{h} + \frac{gh^2}{2}\right]^\top \tag{3}$$

where g = gravitational acceleration [L/T^2].

The source term $\mathbf{S}(\mathbf{U})$ in Eq. (1) can include several physical phenomena. Here, only bed slope and friction effects are considered. Therefore, the source term is

$$\mathbf{S}(\mathbf{U}) = \mathbf{B}(\mathbf{U}) + \mathbf{H}(\mathbf{U}) \tag{4}$$

where $\mathbf{B}(\mathbf{U}, x)$ = bed slope source term; and

$$\mathbf{B}(\mathbf{U}) = \left[0, -gh\frac{\partial z}{\partial x}, -gh\frac{\partial z}{\partial y}\right]^\top \tag{5}$$

where z = bed elevation [L]. Notice that friction acts only for $h > 0$, which points out that friction does not act on vertical surfaces but only on nonvertical surfaces, which are modeled as piecewise constant (horizontal) surfaces represented by the computation cells. Only primary head loss is accounted for by means of Manning's law in the proposed model. Singular or secondary head losses are not included Additionally, in this work the bed may be mobile; therefore, z is a function of time and space $z = z(x, y, t)$. Finally, the friction source term is

$$\mathbf{H}(\mathbf{U}) = [0, -gh\sigma_x, -gh\sigma_y]^\top \tag{6}$$

defined in terms of the directional friction slopes formulated according to the Manning formula:

$$\sigma_x = \frac{n^2 u\sqrt{u^2 + v^2}}{h^{4/3}}$$
$$\sigma_y = \frac{n^2 v\sqrt{u^2 + v^2}}{h^{4/3}} \tag{7}$$

where n = Gauckler-Manning roughness coefficient [$TL^{-1/3}$].

This coefficient is dependent on the bed material. In this work, the movable bed material (i.e., sediment) can be moving over an underlying nonmovable bed material. Therefore, at a particular point in space, the bed material can change in time. Hence, it is

relevant to allow for $n = n(x, y, t)$, depending on the material present at each time, following

$$n = \begin{cases} n_0, & \text{if } h_{sed}(x, y, t) \leq \epsilon_{sed} \\ n_{sed}, & \text{if } h_{sed}(x, y, t) > \epsilon_{sed} \end{cases} \tag{8}$$

where n_0 = roughness coefficient for the nonmovable bed; n_{sed} = roughness coefficient for the sediment; h_{sed} = sediment depth; and ϵ_{sed} = prescribed sediment depth tolerance.

Finally, the system in Eq. (1) requires appropriate initial conditions $\mathbf{U}(x, t = 0)$ and boundary conditions to fully describe the problem.

Movable Bed Model

The evolution of a sediment-like movable bed can be modeled by the Exner equation:

$$\frac{\partial z}{\partial t} + \xi \nabla \mathbf{q}_s = 0 \tag{9}$$

where z = movable bed elevation [L] (and of course the bed for the SWE); $\xi = (1 - p)^{-1}$ = factor dependent on sediment porosity p; and $\mathbf{q}_s = (q_{sx}, q_{sy})$ = bed-load discharge [L^3T^{-1}]. Bed-load discharge is often formulated empirically based on the Grass model (Grass 1983), written as Hudson and Sweby (2003)

$$\mathbf{q}_s = A_g \mathbf{u} \|\mathbf{u}\|^2 \tag{10}$$

where A_g = Grass parameter, which models bed-load transport. Following Murillo and García-Navarro (2010a), bed-load transport can be written as

$$A_g = \frac{\sqrt{g} n^3}{\left(\frac{\rho_s}{\rho_w} - 1\right)\sqrt{h}} K_1 \tag{11}$$

where ρ_s and ρ_w = sediment and water densities [ML^{-3}], respectively; and K_1 = calibration parameter for which a number of different empirical formulations exist. In this work, several formulations of K_1 are explored in the context of a finite-depth sediment layer; they are presented in Table 1.

In the formulas reported in Table 1, r_θ is the ratio

$$r_\theta = \frac{\theta}{\theta_c} \tag{12}$$

where θ = Shields number encompassing the effects of shear stress on the bed:

$$\theta = \frac{\|\mathbf{T}\|}{g(\rho_s - \rho_w) d_l} = \frac{\sqrt{(\rho_w g h \sigma_x)^2 + (\rho_w g h \sigma_y)^2}}{g(\rho_s - \rho_w) d_l} \tag{13}$$

where d_l = mean sediment particle diameter. Here the bed shear stress has been formulated in terms of the friction slopes. Finally, θ_c is the critical Shields number which represents the threshold of sediment motion, related to some critical shear stress $\mathbf{T}_c$. The critical Shields number θ_c is different depending on the empirical formulation chosen, as shown in Table 1.

Although this work aims to study fundamental aspects of 2D numerical simulation of bed-load transport over finite-depth erodible layers, it is relevant to highlight three points in the characterization of the mathematical model considered here. First, alternative formulations to the ones presented in Table 1 exist for bed-load discharge. In particular, in this work the Grass model is used based on its good performance in previous studies (Castro-Díaz et al. 2009; Juez et al. 2013; Hudson and Sweby 2003), except in the first experimental test case, where the bed-load discharge formulation chosen is that suggested by the authors of the experiment. Second, the previous relations as presented in Table 1 are based on an equilibrium bed-load transport criterion; they assume that the total sediment transport adapts to local hydraulic conditions instantaneously—that is, the spatial and temporal delay effects are neglected. Another family of relations is formed by nonequilibrium (or noncapacity) bed-load transport models (Cao et al. 2002; Fernández-Nieto et al. 2014). However, such formulas require a higher number of closure relations for bed sediment entrainment and deposition fluxes, involving much uncertainty. Therefore, in order to diminish such uncertainty, and for simplicity, equilibrium formulas are preferable. Third, the bed-load transport formulas considered in this work have a deterministic nature, although the particles transport is a stochastic process. As stated by Furbish et al. (2012), the bulk sediment transport rate is the sum of the instantaneous sediment transport rate plus the contribution of particle diffusivity. However, because the parametric dependence of particle diffusivity with flow variables is challenging (Bohorquez and Ancey 2015; Heyman et al. 2014, 2016), its contribution to the sediment rate is not considered in this work.

Numerical Model

The underlying solution of the hydrodynamic system [Eq. (1)], required for the solution of the full morphodynamic system, follows Murillo and García-Navarro (2010b). The numerical solution of the complete morphodynamic system defined by Eqs. (1) and (9) follows the scheme proposed by Juez et al. (2014). It is briefly summarized here for the sake of clarity.

The numerical scheme for the water-mass and momentum equations is constructed by defining an approximate Jacobian matrix $\tilde{\mathbf{J}}$ at each edge k between neighboring cells. It is defined based on the normal flux $\mathbf{F}_\mathbf{n}$ (i.e., flux across an edge projected on the vector normal to the edge $\mathbf{n}_\omega$), satisfying

$$\delta \mathbf{F}_{\mathbf{n},\omega} = \tilde{\mathbf{J}}_{\mathbf{n},\omega} \delta \mathbf{U}_k \tag{14}$$

with $\delta \mathbf{F}_{\mathbf{n},\omega} = (\mathbf{F}_j - \mathbf{F}_i) \cdot \mathbf{n}_\omega$, $\delta \mathbf{U}_\omega = \mathbf{U}_j - \mathbf{U}_i$, where $\mathbf{U}_i$ and $\mathbf{U}_j$ = values at cells i and j sharing an edge ω.

From this approximate Jacobian matrix, a set of three real eigenvalues $\tilde{\lambda}^m_\omega$ and eigenvectors $\tilde{\mathbf{e}}^m_\omega$ are obtained, where m spans the vector of conserved variables. The vector of conserved variables, $\mathbf{U}$, is then projected onto the eigenvector basis as

Table 1. Bed-Load Formulas

Name	K_1	θ_c	Reference
AM	$17(1 - r_\theta)(1 - \sqrt{r_\theta})$	0.050	Ashida and Michiue (1972)
EF	$18.74(1 - r_\theta)(1 - 0.7\sqrt{r_\theta})$	0.050	Engelund and Fredsoe (1976)
FLVB	$5.7(1 - r_\theta)^{1.5}$	0.037–0.0455	Fernandez-Luque and Beek (2010)
MPM	$8(1 - r_\theta)^{1.5}$	0.047	Meyer-Peter and Müller (1948)
N	$12(1 - r_\theta)$	0.047	Nielsen (1992)
PE	$11.2(1 - r_\theta^{-1})^{4.5}$	0.030	Parker (1979)
S	$4(d_{90}/d_{30})^{0.2} S_o^{0.6} C(1 - r_\theta)$	0.047	Smart (1984)

$$\delta \mathbf{U}_\omega = \sum_{m=1}^{3} (\tilde{\alpha}\, \tilde{\mathbf{e}})_\omega^m \tag{15}$$

The source terms are also projected onto the eigenvector basis to guarantee the exact equilibrium between fluxes and source terms as follows:

$$[\mathbf{B}(\mathbf{U})_\mathbf{n} + \mathbf{H}(\mathbf{U})_\mathbf{n}]_\omega = \sum_{m=1}^{3} (\tilde{\beta}\, \tilde{\mathbf{e}})_\omega^m \tag{16}$$

With all the necessary information now at hand, the updating of the flow variables in the cell at time t^{n+1} is expressed as

$$\mathbf{U}_i^{n+1} = \mathbf{U}_i^n - \frac{\Delta t}{A_i} \sum_{\omega=1}^{N_\omega} \sum_{m=1}^{3} (\tilde{\lambda}^- \tilde{\alpha} - \tilde{\beta}^-)_\omega^m \tilde{\mathbf{e}}_\omega^m l_k \tag{17}$$

where A_i = area of cell i; l_ω = length of edge ω; and N_ω = number of edges of cell i. The negative superscript $(\cdot)^-$ in Eq. (17) implies that only the incoming waves are considered for updating the flow variables of each cell (upwinding), defining $\tilde{\lambda}^- = 1/2(\tilde{\lambda} - |\tilde{\lambda}|)$. Also, special care is required when computing wet/dry fronts for which the adopted strategy is based on enforcing positive values of water depths at each edge supported by a detailed study of the Riemann problem (Murillo et al. 2009). When these values become negative, the numerical values of the friction and bed-slope source terms are reduced, thus avoiding time step reduction.

In addition, the bed level is updated as follows:

$$z_i^{n+1} = z_i^n - \xi \frac{\Delta t}{A_i} \sum_{\omega=1}^{N_\omega} q_{s,\omega}^* l_\omega \tag{18}$$

Here $q_{s,\omega}^*$ = upwinded bed-load transport contribution of each neighboring cell, across each cell edge ω, following the sign of the approximate characteristic velocity associated with the bed $\tilde{\lambda}_{s,\omega}$ at edge ω separating cells i and j:

$$q_{s,\omega}^* = \begin{cases} \mathbf{q}_{s,i} \cdot \mathbf{n}_\omega & \text{if } \tilde{\lambda}_{s,\omega} > 0 \\ \mathbf{q}_{s,j} \cdot \mathbf{n}_\omega & \text{if } \tilde{\lambda}_{s,\omega} < 0 \end{cases} \tag{19}$$

The characteristic velocity $\tilde{\lambda}_{s,\omega}$ in the so-called weakly coupled scheme proposed by Juez et al. (2014) is not the formal mathematical definition of an eigenvalue of the system, simply because the Exner equation (with which $\tilde{\lambda}_{s,\omega}$ is associated) is not a hyperbolic equation. Instead, and in order to keep a convenient hyperbolic-like formulation, $\tilde{\lambda}_{s,\omega}$ is defined as

$$\tilde{\lambda}_{s,\omega} = \xi \frac{\delta q_{s,\omega}}{\delta z'} \tag{20}$$

Here $\delta q_{s,\omega} = (\mathbf{q}_{s,j} - \mathbf{q}_{s,i}) \cdot \mathbf{n}_\omega$ and $\delta z'$ are defined as

$$\delta z' = \begin{cases} z_j - z_i & \text{if } z_j - z_i > d_l \\ \tilde{\mathbf{u}}\mathbf{n} & \text{otherwise} \end{cases} \tag{21}$$

where $\tilde{\mathbf{u}}\mathbf{n}$ = Roe-averaged velocity at the edge, projected in the direction of the vector normal to the edge.

Regarding the stability criteria, and as stated by Leveque (2002), the explicitly updated conserved variables are defined through the fluxes obtained within each cell. Therefore, the computational time step has to be chosen small enough for ensuring stability. Traditionally, numerical stability has been controlled through the dimensionless CFL (Courant-Friedrich-Lewy) parameter, which takes into account the geometric characteristics of the cells and the hydrodynamic celerities. Following Juez et al. (2014), in the presence of intense bed-load transport the stability criterion is revisited, including the discrete estimation of the bed celerity $\tilde{\lambda}_s$:

$$\Delta t = \text{CFL} \min_{\omega,m} \frac{\chi_\omega}{|\tilde{\lambda}_\omega^m, \tilde{\lambda}_{s,\omega}|} \quad \text{with} \quad \text{CFL} \le 0.5 \tag{22}$$

where χ_ω = relevant distance between neighboring cells (Murillo et al. 2009). With this numerical strategy, the stability condition takes into consideration the most restrictive numerical wave speed coming from both the hydrodynamical and the morphodynamical solvers.

A noteworthy property of this formulation is that, as Eq. (19) shows, the sign of the bed-load transport contributions $q_{s,\omega}^*$ depends on the sign of the velocity vector projected on the normal vector of the edge, not on the sign of the characteristic velocity $\tilde{\lambda}_{s,\omega}$, as is usually true in hyperbolic equations. In this scheme, $\tilde{\lambda}_{s,\omega}$ indicates the direction for upwinding and provides stability guidelines but does not reveal the direction of transport phenomena.

In this work, a GPU implementation of both the SWE solver (Lacasta et al. 2014) and the weakly coupled Exner solver (Juez et al. 2016) has been used. This is particulary useful for the cases computed here because of the large number of repetitions necessary to perform flushing in channels. The cases analyzed have been computed using the Nvidia Kepler-Generation Tesla k40 GPU computing device. As required by the numerical method, double floating-point precision (fp64) is required. This GPU offers 1.4 TFLOPs of throughput on arithmetical calculations in fp64.

Finite-Depth Sediment Layer

In the presence of a physical problem in which the sediment has a finite depth, the Exner equation [Eq. (9)] must be complemented with some constraints to avoid eroding material from a region that is nonerodible. Several conceptual situations can be posed: (1) an infinitely rigid region where no bed evolution can occur; (2) a rigid (clean) bed over which sediment can move; and (3) a sediment layer already lying over a rigid bed that is eventually uncovered. In fact, all three situations are nothing but the same problem of defining constraints to the Exner equation. However, mathematically and numerically it is the third one that is troublesome.

In the first situation of an infintely rigid region, a simple definition of the discrete version of the Grass parameter A_g suffices:

$$A_{g,i} = \begin{cases} 0 & \text{if } h_{sed,i} < \epsilon_{sed} \\ A_g(\mathbf{U}, n) & \text{otherwise} \end{cases} \tag{23}$$

Here $h_{sed} = z - z_o$, with $z_o(x, y)$ the nonerodible surface and ϵ_{sed} a minimum sediment depth tolerance to define a cell as clean or sedimented. In this work, $\epsilon_{sed} = d_{50}$ of the sediment (except where stated otherwise) so that it scales accordingly with sediment properties.

The second case in Eq. (23) is an erodible bed. The first case in Eq. (23) applies when no erodible material is available, which through Eq. (10) results in a particular simplification of Eq. (19):

$$q_{s,\omega}^* = \begin{cases} 0 & \text{if } \tilde{\lambda}_{s,\omega} > 0 \\ \mathbf{q}_{s,j} \cdot \mathbf{n}_\omega & \text{if } \tilde{\lambda}_{s,\omega} < 0 \end{cases} \tag{24}$$

Eq. (24) means that the fix enforced by Eq. (23) acts only on the upwinded contributions and thus no bed material can be removed from the clean cell i but bed material can flow into the cell from cell j (assuming of course that cell j has material). This leads to the second conceptual situation. Once the movable bed material has flowed into an originally nonerodible cell, this

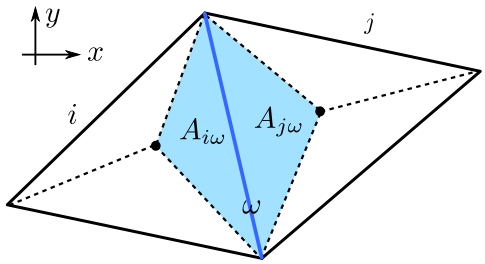

Fig. 1. Edge-relative area fraction for estimating available sediment

cell must be erodible. Eq. (23) allows for this when evaluated at each time step.

Following the same conceptual process, at some time the sediment depth in a particular cell can reduce to $h_{sed,i} = \epsilon_{sed}$, and therefore the first case in Eq. (23) is invoked. However, it is highly unlikely that all nearly clean cells (i.e., cells that can become sediment-free during the current time step) will be eroded exactly to this critical value ϵ_{sed} after updating their states. Many of them will be overeroded, resulting in a negative sediment depth, in a similar way to depth-negativity issues in the presence of wet/dry fronts in water (Murillo et al. 2009). To address this, consider a given time step size Δt^n evolving from time level n to time level $n+1$. A cell will be overeroded if

$$\Delta t^n \sum_{\omega}^{N_\omega} q^*_{s,\omega} l_\omega > h_{sed,i} A_i \tag{25}$$

Therefore, the outgoing (positive) bed-load discharges $q^*_{s,\omega}$ must be limited so as to satisfy

$$\sum_{\omega}^{N_\omega} q^*_{s,\omega} l_\omega = 0 \tag{26}$$

Although this seems straightforward, the problem is that, once Eq. (26) is enforced, a downstream cell j has smaller incoming contributions and might now satisfy Eq. (25). If so, this procedure is applied recursively and there is no guarantee that it will lead to a solution for all cells involved. Furthermore, if there is more than one positive $q^*_{s,\omega}$ contribution in a cell, the problem of how to limit two (or more, depending on cell topology) contributions simultaneously might not have a unique solution.

An alternative approach, based on the principle of mass conservation, is adopted here. As shown in Fig. 1, each cell A_i is divided into subareas, $A_{i\omega}$, which are built by connecting the barycenter of each cell with the vertices of the shaping face ω. Hence, a triangular cell (like the ones considered in this work) is split into three subareas. The corresponding subareas that share a common edge between two elements, A_i and A_j, are denoted $A_{i\omega}$ and $A_{j\omega}$ (Fig. 1).

Thanks to this conservative technique, it is possible to state that the only material available to be transported across edge ω is that inside the fractional subarea $A_{i\omega}$ (assuming that the flow goes from i to j). Therefore, an estimation of the available material from wall ω is

$$V_{i\omega} = h_{sed,i} A_{i\omega} \tag{27}$$

In this way, each contribution $q^*_{s,\omega}$ can be limited independently, based on the maximum available volume for that edge, by enforcing

$$q^{**}_{s,\omega} = \begin{cases} C \dfrac{V_{i\omega}}{\Delta t^{n-1} l_\omega} & \text{if } q^*_{s,\omega} \Delta t^{n-1} l_\omega > V_{i\omega} \\ q^*_{s,\omega} & \text{otherwise} \end{cases} \tag{28}$$

Here the coefficient $C \lesssim 1$ accounts for two effects. The first is that the subareas $A_{i\omega}$ are only approximations of the real contributing areas to the flux on that edge. Clearly, the geometry-based partitioning of the cells does not necessarily reflect the real contributing areas, which are flow-dependent. However, the subareas strategy helps in estimatingthe material available to be eroded by limiting the possible mismatch. The second effect is that the corrected contributions $q^{**}_{s,\omega}$ update the cells with a time step Δt^n. This time step size is unknown when Eq. (28) is evaluated; only the previous time step size Δt^{n-1} is known. Therefore, $C \lesssim 1$ helps in avoiding problems when $\Delta t^n > \Delta t^{n-1}$, which has often been observed.

Furthermore, if $\Delta t^n \gg \Delta t^{n-1}$, the correction enforced by Eq. (28) might still not be sufficient and a cell might still be eroded below the rigid surface elevation. Two issues arise concerning this possibility. The first, again, is that Δt^n cannot be computed until after computing all contributions edgewise. The second is that the problem cannot be identified until the cells are updated (cellwise) with the (already computed) edge contributions. One possibility would be to act on the edge contributions yet again, but the potential pitfall is that downstream cells could now have issues. The adopted alternative idea, which is much more aggressive, is to simply truncate the maximum time step size, which avoids overerosion in the computational domain. This is done by testing, cellwise, if the sediment depth (resulting from adding the flux contributions to each cell) is negative. If so, the time step is reduced to half its size, the flux contributions are again added (over half the time step), and the evaluation of the resulting sediment depth is repeated recursively until it is nonnegative (in practice, it is checked that $h_{sed} > -0.01\epsilon_{sed}$, which is somewhat more relaxed than $h_{sed} > 0$).

Validation Tests

In order to test the method and its implementation, and to assess both the applicability and efficiency of the proposed strategy, two test cases are studied. Both are 1D laboratory flume experiments in which the sediment can be eroded to expose a nonerodible bed. The first case deals with a slowly evolving flow; the second, with violent flushing flow conditions.

Test Case 1: Experimental Straight Flume with Nonerodible Layer

A laboratory test case carried out by Struiksma (1999) is here reproduced by means of the proposed numerical method. It consists of a straight channel of length 11.5 m and and width 0.2 m. The channel has a fixed and nonerodible layer approximately 3 m long located in the middle of the flume. The channel is also filled with rather uniform sand ($d_{50} = 0.45$ mm, $d_{90} = 0.6$ mm) conforming to an erodible stratum and defining the initial sediment surface. This is a suitable case for benchmarking because theexperimental results are available and have been numerically reproduced before (Ortiz et al. 2015; Rulot et al. 2012; Struiksma 1999). The case consists of sustained steady flow with recharging sediment in the upstream boundary. Fig. 2 shows the two initial sediment profiles considered in this work {hereafter C1 [Fig. 2(a)] and C2 [Fig. 2(b)]}. A 4-cm-deep and 2-m-long trench is initially excavated in both layouts. This trench moves with the flow, at some point exposing the underlying nonerodible stratum. This is the process of particular interest.

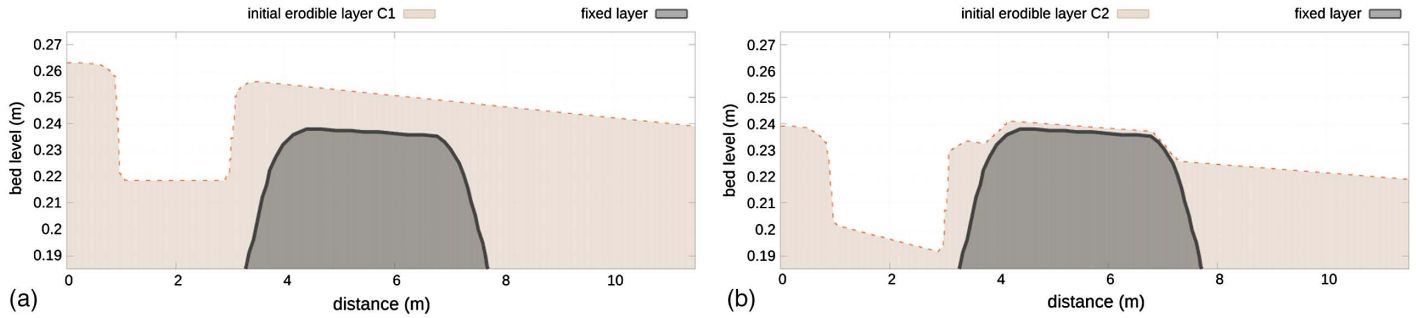

Fig. 2. Initial sediment profiles and nonerodible layer for Case 1: (a) C1; (b) C2

A steady discharge of 9.2 L/s is introduced into the system as the inlet boundary condition [Fig. 2(a)] and a fixed water level is imposed as the outlet boundary, with $h + z = 0.338$ and $h + z = 0.323$ m for C1 and C2, respectively [Fig. 2(b)]. Because water and sediment were both recirculated in the original experiment, periodic boundary conditions are set in the simulations. According to Struiksma (1999), an equivalent Manning roughness coefficient of $n = 0.022$ sm$^{-1/3}$ was selected, corresponding to a Chézy coefficient of $C = 31.5$ m$^{1/2}$ s^{-1}. In this experimental test case, the Grass model for bed-load transport is not used. Instead, and for the sake of consistency, the empirical bed-load transport formula proposed by Struiksma (1999) is used:

$$\mathbf{q}_s = \kappa \mathbf{u} \|\mathbf{u}\|^4 \tag{29}$$

Different values for the coefficient κ in Eq. (29) in each layout have been chosen: $\kappa = 3.2 \times 10^{-4}$ s^4/m^3 in C1 and $\kappa = 2.7 \times 10^{-4}$ s^4/m^3 in C2. According to Struiksma (1999), κ is an adjustable parameter for reproducing the propagation of the front of the trench. These values are not exactly the same as those reported by Struiksma (1999). Given that a different numerical method and a different framework (1D versus 2D) is used here, it is expected that values might need recalibration. The values are on the same order of magnitude as in (Struiksma 1999) although somewhat lower for the second configuration (as expected, because the nonerodible layer in the second configuration is exposed longer than in the first configuration). Again, for this particular case the sediment depth tolerance is set to $\epsilon_{sed} = 6 \times 10^{-3}$ for C1 and to $\epsilon_{sed} = 3 \times 10^{-3}$ for C2.

Both configurations are simulated on a triangular unstructured mesh composed of 7,218 cells and 4,020 nodes. A detailed view of the mesh is shown in Fig. 3. Case C1 is run until and Case C2 until $t = 36{,}000$ s, which are the latest reported experimental results (Struiksma 1999). The numerical results and the experimental measurements are compared in the form of a longitudinal profile along the centerline ($y = 0.1$ m) of the channel at different times in Figs. 4(a and b) for the C1 and C2 configurations, respectively. Only the first 5 h are plotted for C1. The numerical results provided by Struiksma are also included for the sake of completeness.

As Fig. 4 shows, the trench evolution is well captured during the entire process for both layouts, reproducing well the advance of the sediment front. However the simplified solid transport formula used does not allow accurate simulation of the behavior on top of, just before, and after the fixed layer, resulting in an overestimation of the erosion near the nonerodible bump. The results particularly relevant to this study are these: first, the simulation remains stable when the erodible material is removed; second, the nonerodible layer can be exposed accurately; and third, because of the steady inflow (water and sediment), there is always more incoming sediment that can re-cover the nonerodible layer. This means that the nonerodible layer can be re-exposed. This process triggers the sediment-depth-positivity conditions many times during the simulation and often effectively reduces the time step to ensure numerical stability. This is the reason that the computational effort (in terms of GPU time) for these simulations is rather large for a one-dimensional case: 2.05 h for C1 and 3.33 h for C2.

The root-mean-square error (RMSE) of both numerical results with respect to the experimental measurements is shown in Table 2. The results obtained with the scheme proposed in this paper are labeled *Simulated*. The overall results show that in terms of RMSE the models are comparable. The results by Struiksma (1999) are arguably marginally better but show no clear trend.

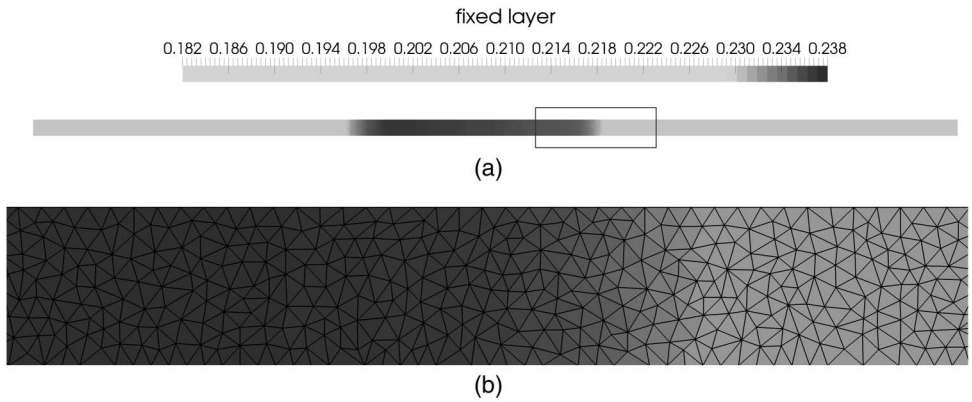

Fig. 3. (a) Nonerodible bed elevation for the entire channel; (b) detailed view of the mesh downstream of the nonerodible step

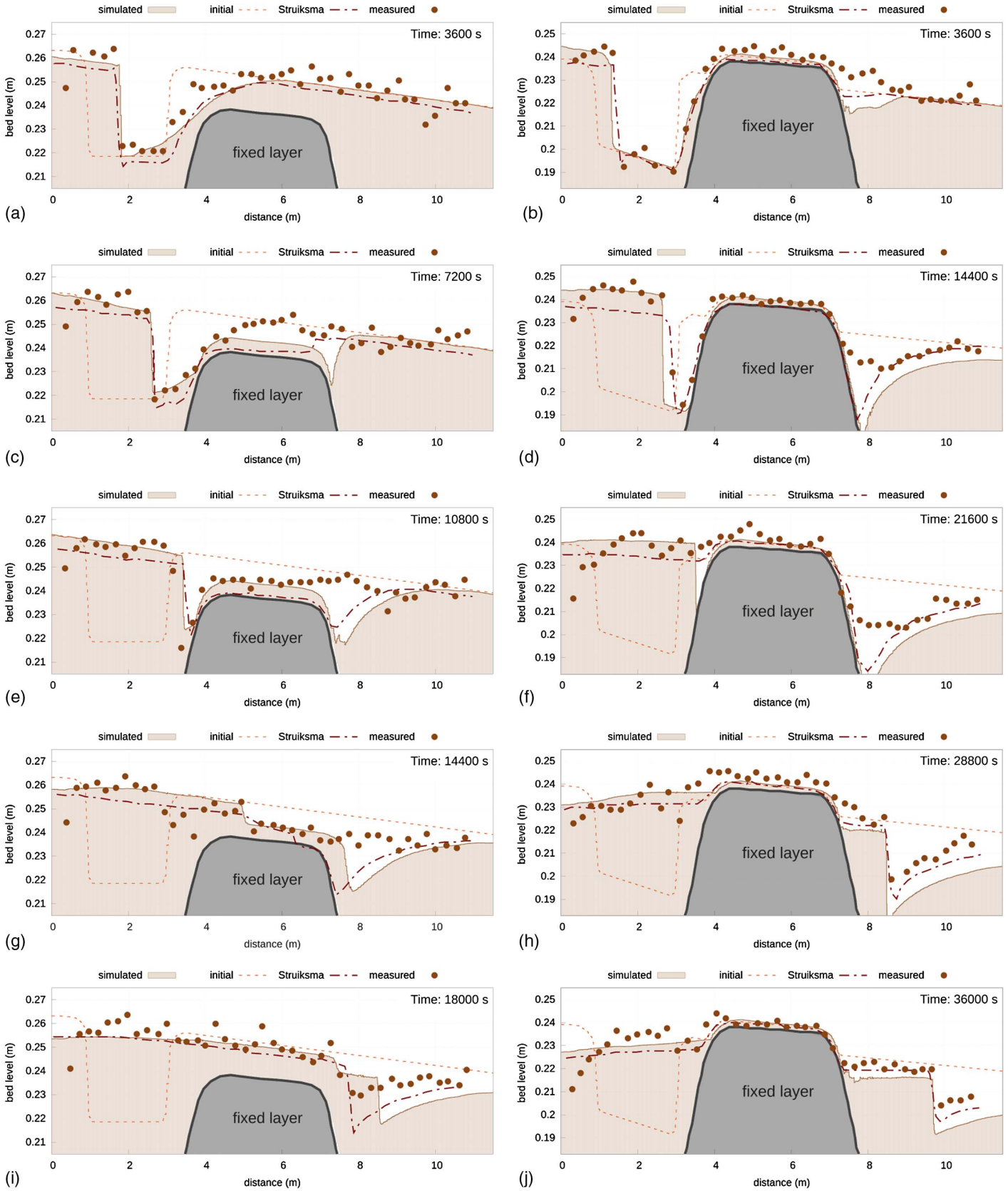

Fig. 4. Sediment distribution for configurations C1 (a, c, e, g, i) and C2 (b, d, f, h, j) at different times

The comparison can be further assessed by qualitatively comparing the profiles shown in Fig. 4, where the numerical profiles are similar. In general terms, they both underestimate or overestimate the sediment elevation in the same way when compared with experimental results. Notable differences occur in C1 at $t = 18{,}000$ s, where Struiksma's (1999) results show a single sharp front whereas the solution computed with the proposed algorithm shows two successive sediment fronts.

Table 2. RMSE of Experimental Data for the Presented Numerical Model and the Struiksma Formulation

Case	Time (s)	RMSE simulated (m)	RMSE Struiksma (m)
C1	3,600	$\mathbf{6.419 \times 10^{-05}}$	5.259×10^{-04}
	7,200	$\mathbf{9.963 \times 10^{-04}}$	1.452×10^{-03}
	10,800	$\mathbf{7.366 \times 10^{-04}}$	1.022×10^{-03}
	14,400	4.095×10^{-04}	$\mathbf{1.995 \times 10^{-04}}$
	18,000	1.616×10^{-03}	$\mathbf{6.158 \times 10^{-04}}$
C2	3,600	$\mathbf{1.746 \times 10^{-04}}$	2.872×10^{-04}
	14,400	5.579×10^{-04}	$\mathbf{3.339 \times 10^{-04}}$
	21,600	1.058×10^{-03}	$\mathbf{3.182 \times 10^{-04}}$
	28,800	1.818×10^{-03}	$\mathbf{8.294 \times 10^{-04}}$
	36,000	1.692×10^{-03}	$\mathbf{8.125 \times 10^{-04}}$

Note: Best RMSE for each time is highlighted in bold.

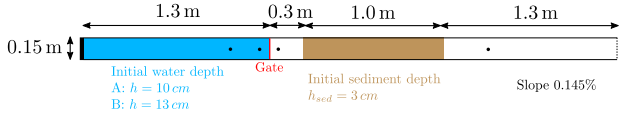

Fig. 5. Experimental setup of the flushing experiment

Test Case 2: Experimental Flushing Channel

Campisano et al. (2004) reported a 1D flushing experiment on a laboratory channel. The setup is shown in Fig. 5 in plan view. The flume, 3.9 m long with a rectangular cross section 0.15 m wide, was set with a slope of 0.145%. A gate was placed at $x = 1.3$ m from the upstream end. The upstream boundary ($x = 0$) was closed, and the downstream boundary ($x = 3.9$) was left as a free fall into a sediment trap. A 1-m-long, 3-cm-thick sediment layer was laid downstream from the gate as shown in the figure. The flume material was plexiglass and therefore nonerodible. Four pressure probes (shown as black dots in Fig. 5) were placed at $x = \{0.6, 1.20, 1.40, 3.30\}$.

An initially hydrostatic water volume was set upstream of the closed gate. Two experiments were performed. Following the notation of Campisano et al. (2004), the initial hydrostatic conditions satisfied $A := h(x = 1.3, t = 0) = 0.1$ and $B := h(x = 1.3, t = 0) = 0.13$ m. At $t = 0$ s, the gate was opened (and assumed to open instantly) and a dam-break wave propagated downstream, mobilizing the sediment. The experiment continued until all water had flowed out of the channel. Then the gate was closed and the upstream reach was refilled with water to the same initial condition. The experiment was then repeated. The process was repeated for as many cycles as necessary to completely remove the sediment from the channel.

The computational mesh was a 2D unstructured triangular mesh with 35,075 cells. The domain extended beyond the downstream end of the flume in order to collect the sediment as in the experiment. Therefore, the computational downstream boundary was also closed to form a sediment trap.

For calibration purposes, Campisano et al. (2004) reported the time evolution of water depth recorded by the four pressure probes in a case without any sediment. This was designed to validate their 1D hydrodynamic model. According to Campisano et al. (2004), $n_\sigma = 0.0105$ sm$^{-1/3}$. Using this value, simulations with Initial Conditions A and B were performed. In this work, these two tests werre used to calibrate the Gauckler-Manning coefficient of the nonerodible channel bed. Results are shown in Fig. 6, in red,

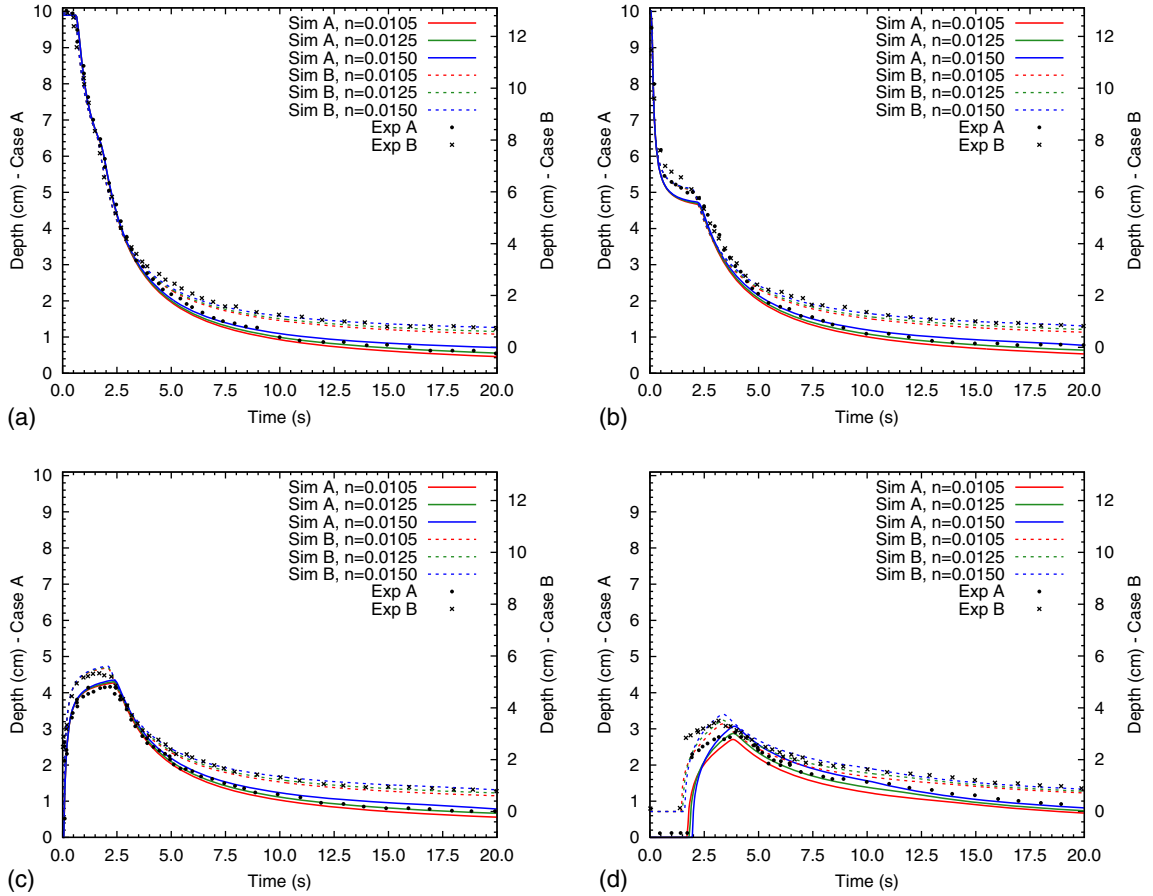

Fig. 6. Water depth evolution of the dam-break test without sediment: (a) $x = 0.6$; (b) $x = 1.2$; (c) $x = 1.4$; (d) $x = 3.3$

J. Hydraul. Eng., 2017, 143(9): 04017034

for three Gauckler-Manning coefficient values. The figure shows that the hydrodynamic simulation results in a better fit for $n_\sigma = 0.0125$ sm$^{-1/3}$ in both Case A and Case B. The reason for this higher value of the Gauckler-Manning coefficient than the one reported by Campisano et al. (2004) is that in the 2D model friction effects are only accounted for at the bed whereas in physical reality, and in a 1D formulation, the entire wetted perimeter contributes to friction. Because the experiment takes place in a laboratory flume, it is reasonable that the wetted-perimeter (P) is significantly larger than the width (B): $P = B + 2h > B$. That is, the 1D formulation has a larger area contributing to friction for the same depth and velocity, and therefore the 2D model requires a somewhat higher roughness that the one calibrated for the 1D computations by Campisano et al. (2004). Fig. 6 corroborates that a calibrated roughness coefficient in this bed-only friction representation is sufficient for this test.

At this point, with a calibrated hydrodynamic setup, flushing simulations were performed. Sediment properties (following the experimental report) were set as follows: $\rho_s = 2{,}830$ kg/m^3, $p = 0.65$, $d_{50} = 0.5$ mm. The Gauckler-Manning coefficient for sediment-covered areas was set to $n_\sigma = 0.01334$ sm$^{-1/3}$ following the value reported by Campisano et al. (2004). Sediment-based friction only occurs at the bed, not on the sides. Therefore, the correction to roughness necessary for the plexiglass channel was not necessary for the sediment.

Fig. 7 shows the evolution of the simulated and experimental flushing efficiency, defined as

$$\eta_v = \frac{V_s(t=0) - V_s(t)}{V_s(t=0)} \tag{30}$$

where V_s = sediment volume; and t = time. Note that $\eta_v = 0$ initially and, as time and flush cycles advance, $\eta_v \to 1$. Full cleansing of the channel is achieved when $\eta_v = 1$. Experimentally, Case A results in a clean channel after 25 flushes; Case B, after 15 flushes. Numerical results are summarized in Fig. 7(a) for Case A and in Fig. 7(b) for Case B. These figures include experimental efficiencies and the efficiencies obtained from the numerical results reported by Campisano et al. (2004). The figures show a shaded region that indicates the envelope of the numerical results obtained by Campisano et al. (2004).

Fig. 7(a) shows that all bed-load transport formulas underestimate flushing capacity in Case A. The best results are obtained by EF and N. Importantly, EF almost achieves complete flushing by the 25th cycle. Both EF and N slightly underestimate flushing capacity throughout the process, but show the same trend (i.e., similar slope) as the experimental results. In contrast, all other formulas show a significantly lower slope and thus growing discrepancies. Fig. 7(b) shows that full flushing in Case B is nearly obtained by 15 flush cycles for the EF, N, and AM formulas only. All other bed-load formulas drastically underestimate the flushing capacity. Of the three formulas that do perform well, EF overestimates the flushing efficiency throughout the entire process. In fact, it shows little variations in flushed volume after the 13th cycle. In contrast, N systematically underestimates the flushing capacity, but still shows flushing evolution until the 15th cycle, when flushing variations should stop. The AM formula also underestimates flushing capacity and fails to achieve near full flushing at 15 cycles, but achieves it by the 16th cycle. Together, the flushing efficiency results in Fig. 7 show that EF and N are reasonable choices and seem to perform better for more energetic flows.

When comparing the results from these simulations with those obtained by Campisano et al. (2004), it is observed that only EF, N, and AM fall in the same range of efficiency. All others fall much below the worst predictions by Campisano et al. (2004). In Case A, EF and N are similar to the best results by Campisano et al. (2004). In Case B, results obtained with N, EF, and AM are similar to the best results by Campisano et al. (2004). It is noteworthy that Campisano et al.'s (2004) results always underestimate cleaning efficiency. However, in Case B the EF formula overestimates it and the N formula slightly outperforms the trend reported by Campisano et al. (2004).

Table 3 shows the RMSE for both cases and all transport formulas used, relative to the experimental measurements. It also includes the RMSE for the best and worst results from the original simulations by Campisano et al. (2004) for comparison. The RMSE in Table 3 is in terms of volumetric cleaning efficiency units. The table quantitatively shows that the most accurate performance, on average, is obtained with the EF formula in both cases. In Case A, both N and EF are within the results obtained by Campisano et al. (2004). Interestingly, AM does not fall within the RMSE range, although it graphically falls between the efficiency curves from

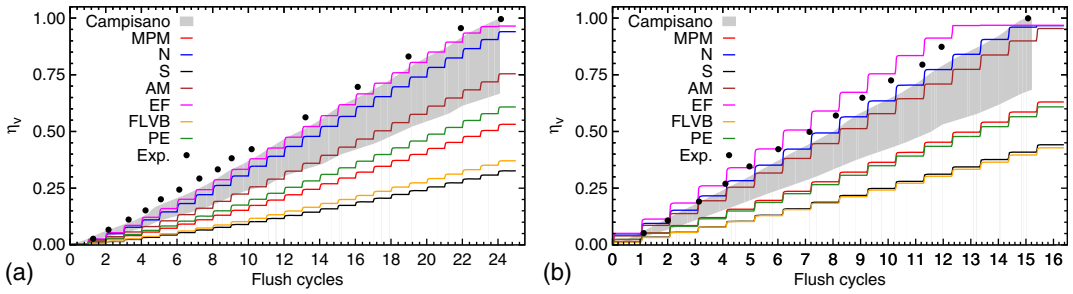

Fig. 7. Flushing efficiency for the experimental case: (a) Case A; (b) Case B

Table 3. RMSE (in Terms of Efficiency) of All Transport Formulas in the Flush Experiment and the Struiksma Formulation

	Formula						Campisano et al. (2004)		
Case	MPM	N	S	AM	EF	FLVB	PE	Minimum	Maximum
A	0.0691	0.0212	0.0918	0.0442	**0.0135**	0.0869	0.0607	0.00463	0.0255
B	0.0755	0.0154	0.1034	0.0264	**0.0069**	0.1051	0.0790	0.0066	0.0297

Note: Best RMSE for each time is highlighted in bold.

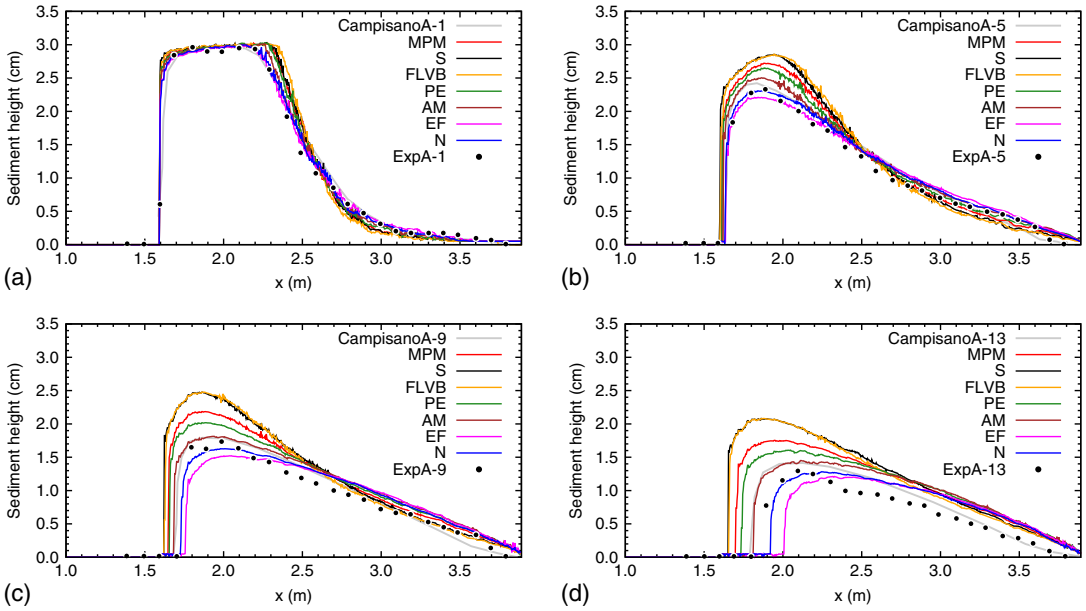

Fig. 8. Sediment depth profiles for Case A after several flush cycles: (a) Flush 1; (b) Flush 5; (c) Flush 9; (d) Flush 13

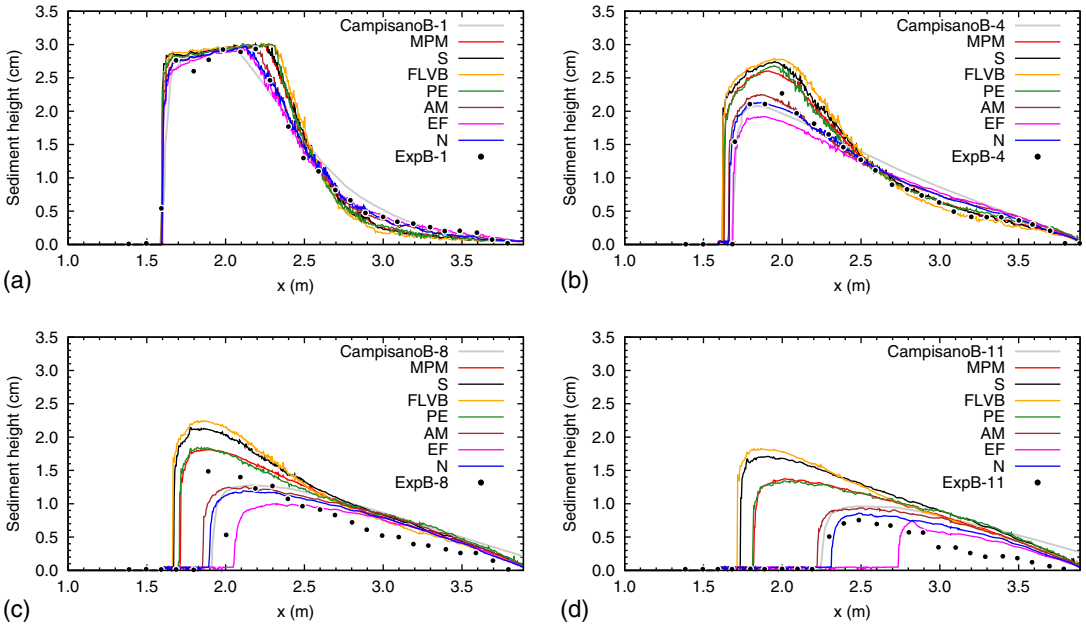

Fig. 9. Sediment depth profiles for Case B after several flush cycles: (a) Flush 1; (b) Flush 4; (c) Flush 8; (d) Flush 11

Campisano et al. (2004), suggesting that the RMSE does not provide a full picture of performance for this analysis and that the graphical information from Fig. 7 must not be overlooked. In Case B, EF also outperforms Campisano et al.'s (2004) best result and N and AM closely follow within the range of the original numerical results. All other formulas underperform Campisano et al.'s (2004). simulations

Figs. 8 and 9 show simulated and experimental results after several flush cycles (for which experimental results are available) for Cases A and B, respectively. They also include the numerical results reported by Campisano et al. (2004) using the MPM formula for Case A and the Kalinske (1947) formula for Case B, which yielded the best results in their simulations.

As expected from the results in Fig. 7, overall the EF, N, and AM formulas yield the best results. There is an interesting evolution that is worthy of discussion. After the first flush cycle, all formulas yield similar results, although two groups are clearly distinguishable. The first group is EF, N, and AM, which manage to fit the profile approximately in all three identifiable regions: step and plateau ($x \leq 2.2$), high slope ($2.2 \leq x \leq 2.8$), and mild slope ($x \geq 2.8$). The second group, MPM, S, FLVB, and PE, only fits well in the step and plateau. It underestimates erosion in the high slope region and therefore underestimates the sediment depth in the mild slope region, where the material should have remained. After 5 (Case A) or 4 (Case B) flush cycles, the two groups are very much apart. The first group reproduces the profile reasonably well, with overestimation of the depth in the region $x > 2.5$, which is now almost a constant slope (instead of two slopes). The AM and N formulas outperform EF. The second group fails to capture the maximum depth, but approximates better the slight curvature

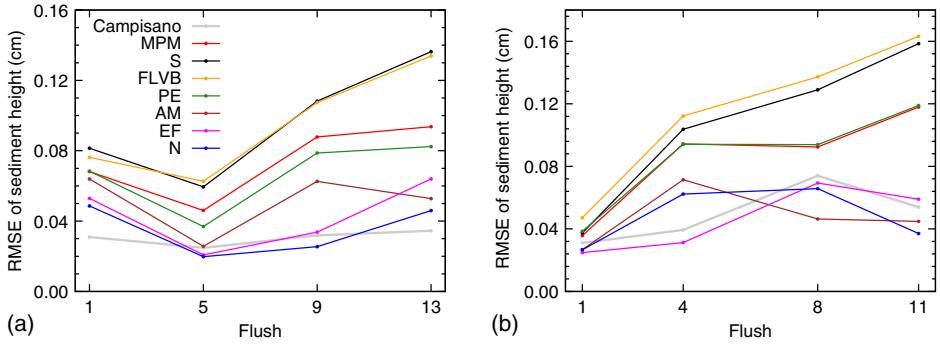

Fig. 10. RMSE of sediment profiles: (a) Case A; (b) Case B

present in $x > 2.5$. However, by 9 (Case A) or 8 (Case B) and later 13 (Case A) or 11 (Case B) flush cycles, it is very clear that the second group drastically underestimates bed-load transport whereas the first group performs much better. In particular, after 13 (Case A) or 11 (Case B) cycles, it is clear that the best fit is obtained with the N formula. The AM formula underestimates bed-load transport, and the EF formula is too optimistic. It is also clear that, as the layer becomes thinner, accuracy is reduced. This is likely due in large part to the underlying issue of dealing with very small height sediment layers.

The sediment profiles from N, EF, and AM are similar to those obtained by Campisano et al. (2004). For better comparison, Fig. 10 summarizes the RMSE of the sediment profiles, including the results by Campisano et al. (2004). The figure shows clearly that MPM, S, FLVB, and PE result in growing error as more flushes are performed. Fig. 10(a) shows that the Nielsen formula results in the best profiles, with errors comparable to those of Campisano et al. (2004). In Case B, as Fig. 10(b) shows, N, EF, and AM provide similar results. Which is best depends on the flush cycle that is observed. By the end of the flushing process, the N formula results in the smallest errors, slightly outperforming Campisano et al. (2004). Another interesting behavior observed in Fig. 10 is that, for the formulas that yield acceptable results (EF, N, and AM), the error is nonmonotone. This suggests that model performance is dependent on the bed and its dynamics.

From the overall analysis of efficiency indicators and the errors in the sediment profile, it follows that the Nielsen formula yields the best results for this type of flushing process. The N formula results in the correct trend of sediment flushing and the best sediment profiles.The EF formula is a suitable alternative and perhaps better than N for less energetic flows (Case A). Furthermore, from a hydraulic design point of view, if the goal of a simulated flushing process is to determine the flushing capacity of a particular setup, the tendency of EF to overestimate flushing capacity also suggests that the Nielsen formula is a conservative choice. Finally, in terms of computational effort, the required GPU time for these simulations is approximately 4 min per flush, varying somewhat on the bed-load formulation.

Application Test

This section presents one type of application to which the numerical scheme described in this work is particularly relevant and suitable. This is the case of channel flushing. The test case presented here is an underground stormsewer tank to be constructed in Bilbao, Spain. The tank is designed to perform as a stormwater buffer between the stormsewer collection system and a water treatment plant. Water is expected to carry sediments as bed-load transport into the tank. If the conditions are such that the tank must act as a buffer, a gate downstream is closed and water is retained in the tank with zero velocity, perhaps for days. Therefore, substantial sedimentation both of bed-load transport and suspended sediment is expected. Here, an application of the proposed model to the analysis of flushing scenarios for this tank is presented The goal is twofold: first, to assess if the numerical scheme can properly handle the high-energy, highly erosive conditions that can happen during flushing events in real scale (in addition to the small-scale experiment shown in the previous section); second, to assess the applicability of such a computational tool to engineering analysis, in particular flushing scenarios with large gaps in the scale of geometry and the scale of sediment masses.

The tank is essentially a 1.24-km-long concrete tunnel with three distinct reaches. The upstream reach (UR) is a storage tank for flushing with a fast-opening gate at its downstream end. The middle reach (MR) is the bulk of the tunnel, and the downstream reach (DR) is a transition into a smaller pipe that leads to the water treatment plant. The first two reaches have a bed slope of 0.826%, and the downstream reach has a slope of 3%. Each reach has different cross-sectional geometry, as shown in Fig. 11. The cross sections follow the design of the structure. Between UR and MR lies the gate structure, and between MR and DR lies a transitional region with a rather complex geometry. As is clear in Fig. 11, the cross sections are closed polylines, which of course cannot be represented in a 2D model; only the bed elevation of the channel (dark in Fig. 11) is represented in the 2D computational domain shown in Fig. 12. The computational mesh is an unstructured tessellation of 127,516 triangular cells. Mean cell area is 0.115 m^2, minimum cell area is 0.01 m^2, and maximum cell area is 0.2 m^2. The region around the gate, the region around the transition from MR to DR, and the region containing the contraction and pipe are further refined. In such regions, the mean cell area is 0.033 m^2. In the MR, the tunnel cross section is spanned by approximately 50 cells,

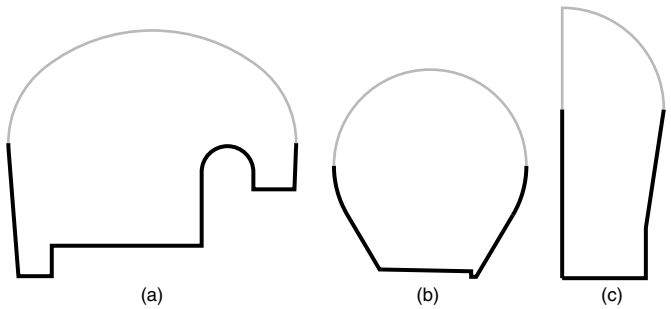

Fig. 11. Cross sections of stormsewer tank: (a) upstream reach; (b) middle reach; (c) down stream reach

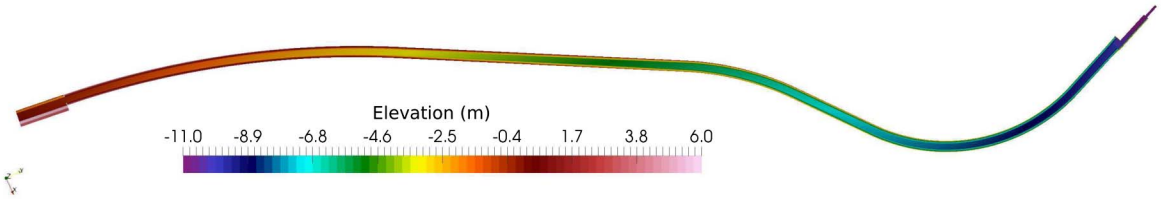

Fig. 12. Computational mesh for stormsewer tank

whereas the tunnel cross section immediately downstream of the gate is spanned by approximately 95 cells.

The sediment selected for the numerical study has the following properties: density $\rho_s = 2{,}650\ \mathrm{kg\,m^{-3}}$; particle size distribution $d_{30} = 0.3$, $d_{50} = 1.0$, and $d_{90} = 10$ mm; porosity $p = 0.40$; and critical Shields number $\theta_c = 0.047$. The Nielsen formulation (Nielsen 1992) is used because it proved to be accurate in the previous experimental case. The Glaucker–Manning roughness coefficient for the sediment is computed as (Meyer-Peter and Müller 1948)

$$n = \frac{d_{90}^{1/6}}{26} = 0.0178\ \mathrm{sm^{-1/3}} \tag{31}$$

For exposed concrete, the coefficient is set to $0.013\ \mathrm{sm^{-1/3}}$. Although the tank is fundamentally a channel, for most of its length (i.e., middle reach with tunnel cross section) the wetted perimeter can be well approximated by the channel bed, considering that the side slopes are represented in fact as part of the bed in the 2D representation. It is only in the DR, where actual vertical walls occur, that the wetted perimeter can be somewhat poorly represented.

Flushing in the tank is controlled by a fast-opening gate between the upstream and middle reaches, with dimensions of 6×1 m, and is assumed to go from closed to fully open at a constant rate in 5 or 10 s. The numerical representation of the time-dependent gate opening is described by Morales-Hernández et al. (2013). The domain is closed in all boundaries except the downstream boundary, where the tunnel physically connects to a pipe. The pipe is not represented in full, and therefore a free outflow boundary is set.

The initial conditions for the flushing events are assumed as follows. For the initial state of water, all of the tank, with the exception of the UR, is dry. The UR holds water for flushing, and three water heights (at the gate) are considered: 10, 8, and 6 m (Cases A, B, and C for gate openings of 5 s; Cases D, E, and F for gate openings of 10 s) to observe the influence of this operational condition on flushing capacity. Initial conditions for the sediment assume that the sediment lies only on the channel bottom, not on the slopes, and is uniformly distributed along the middle and downstream reaches. Initial sediment heights from 0.5 to 10 cm were tested to observe the influence of the initial deposits on the flushing capabilities. The cases are named according to the initial height in centimeters; for example, Case A3 is Case A with 3 cm of initial sediment height. The exceptions are 0.5 and 0.7 cm, which are referred to as 05 and 07, respectively.

Every flushing event consists of three cycles. Cycles start when the gate is opened and finish when water has completely left the domain. Then the initial condition for water is reset and a new gate opening follows. Overall, 108 simulations (cycles) were performed. The simulation time for each cycle was set to 2,600 s, which was tested to be sufficient, and computed with CFL ≤ 0.7.

The transient, 2D results for all simulations are similar. For illustrative and discussion purposes, a few results are reported here. Figs. 13 and 14 show results of the depth (above), velocity (middle), and sediment height (bottom) fields.

Fig. 13 shows the evolution of the first minute for Case D3 in the upstream reach and approximately the first third of the middle reach. In the figure, the formation of two dimensional patterns is clear, including the supercritical reflections of the channel side slopes. More important, it is seen how, for an initial depth of 3 cm, the initial dam-break phenomenon is able to expose the channel bottom.

Fig. 14 shows the evolution of the 2D fields in the DR. This reach shows a complex evolution, starting from an initial impact at $t = 230$ s evolving into a supercritical jet with reflections at $t = 240$ s. The water then reaches the abrupt contraction that leads into the pipe, creating a backwater effect that results in a drastic drop in velocity. After this, the water slowly drains out. In terms of flushing, it is particularly noteworthy that the jet flow at $t = 240$ s

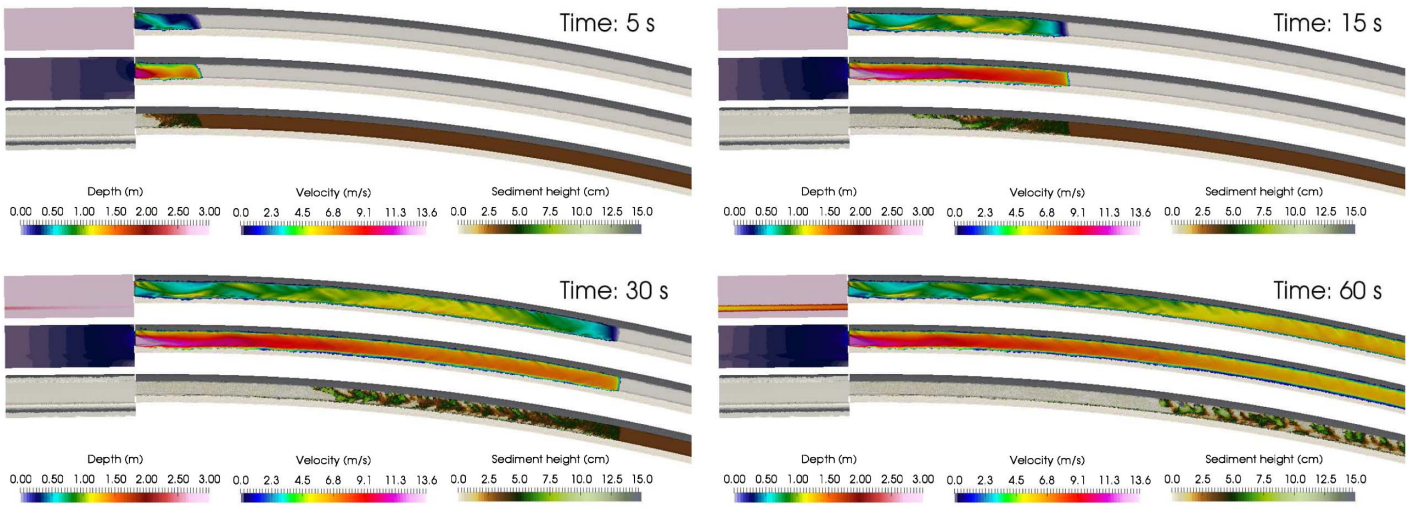

Fig. 13. Upstream reach evolution—Case D3

J. Hydraul. Eng., 2017, 143(9): 04017034

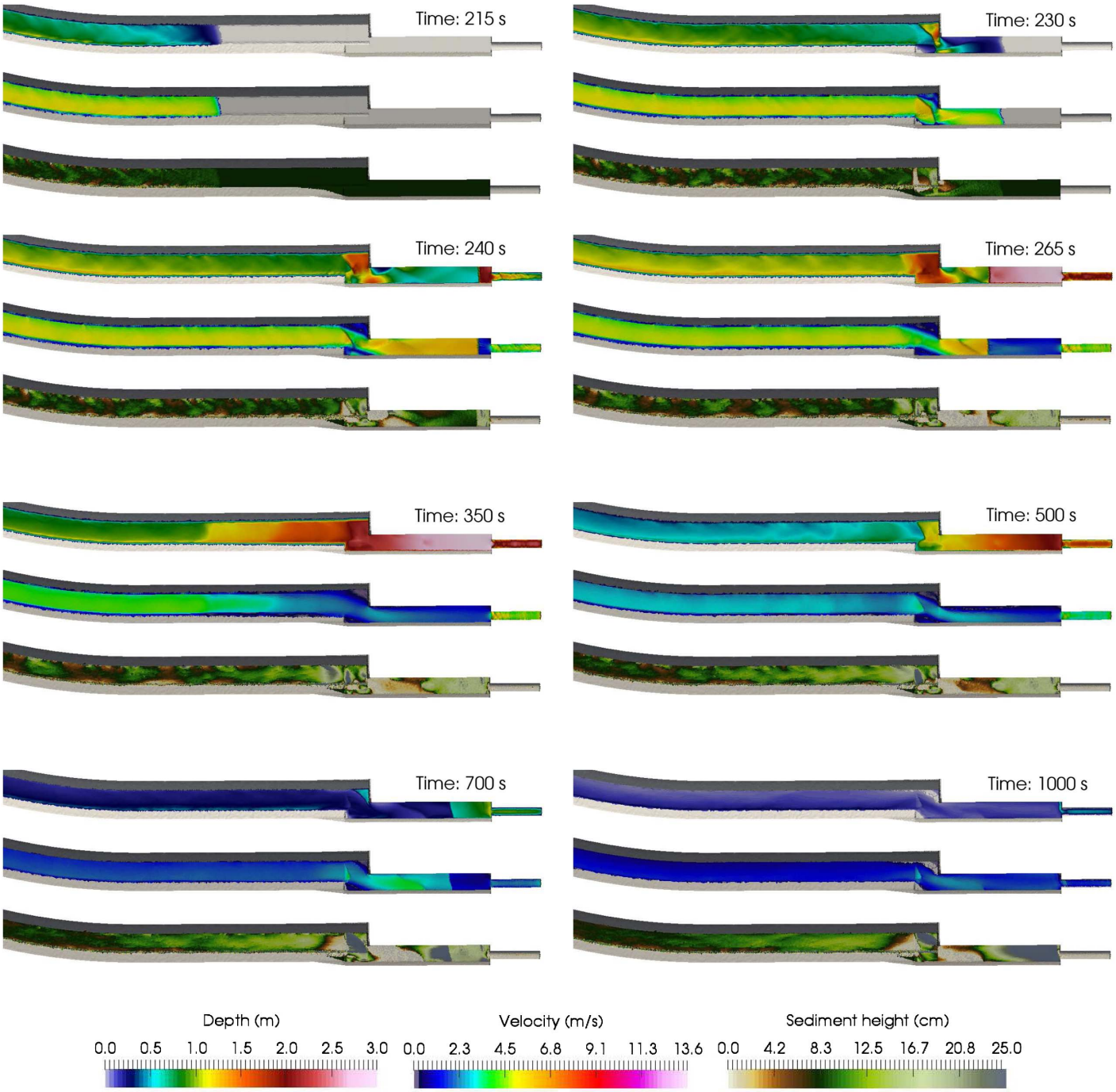

Fig. 14. Downstream reach evolution—Case A8

creates some recirculation and preferential flow paths, thus leading to a large transport capacity in the jet and sedimentation regions in the recirculation zones. The sediment is transported into the contraction, but the sudden drop in velocity creates an immediate loss in transport capacity. Thus, sediment is deposited upstream of the pipe. Feedback is created because the bed elevation rises as sediment is collected at this location, further lowering velocity and favoring more sedimentation. By the time the backwater effect recedes, the established draining flow has a lower transport capacity than that of the initial wave. The overall effect is that, although the flushing cycle might result in significant cleanness upstream, a large part of the sediment does not leave the tunnel because of the sediment trap created by the geometry. The evolution in this region explains why the sediment does not exit the domain and clearly shows the relevance of 2D simulation in this context. The behavior of this reach also suggests that it may be plausible and perhaps even more efficient to use prolonged inflow hydrographs for flushing the sediment because the backwater effect can be avoided and the transport capacity optimized, particularly in the downstream reach.

In this test, friction can be affected by poor representation of the wetted perimeter. Figs. 13 and 14 broadly show the magnitudes of the hydraulic variables that are useful in assessing the validity of modeling friction only on bed surfaces, without considering lateral surface friction in channel flows such as in this case. From Fig. 13, it can be observed that water depth is at peak at approximately 1.5 m, which means that the wetted perimeter in the tunnel cross section is mostly the channel bed, which has a width of

approximately 6 m plus somewhat less than 1.5 m of each side slope region, which also contributes to the numerical simulation. This shows that the wetted perimeter and friction are well estimated. If the depth were significantly greater, the wetted perimeter might be poorly estimated, thus underestimating friction. In the DR, high water depths (up to 2.5 m) develop because of the backwater effect created by the sudden contraction near the downstream boundary. This high water depth, together with the vertical walls in this reach, suggests that the wetted perimeter may be poorly estimated in this region, and that the friction effects may be underestimated. However, because velocity is not very high (on the order of 1 m/s) in this region, and mainly because the flow appears to be controlled by the backwater effect, friction errors are not expected to introduce significant differences in the bulk of the flow. Furthermore, recalling that the roughness coefficient for the sediment is approximately 36% higher than that of the exposed concrete, and given that the sediment is mostly in the center of the channel (that is, in the channel bed, not the side slopes), it is expected that for most of the tank, in the presence of sediment, the channel bed mostly contributes to friction. In summary, although friction might be locally underestimated, the errors in friction estimation should not compromise the reliability of the simulations.

To summarize the results, a flushing efficiency analysis is performed. However, because a large part of the sediment does not leave the domain, instead of analyzing the sediment volume, the efficiency is quantified in terms of clean area:

$$\eta_a = \frac{A_c(t)}{A_T} \tag{32}$$

where $A_l(t)$ = exposed concrete area in the middle and downstream reaches (where *clean* means $h_{sed} < d_{50}/10$); and A_T = total area of the middle and downstream reaches. Clearly, if $\eta_a = 1$, all sediment has been removed. Initially $\eta_a > 0$ becausenot all of the channel bed is assumed to be covered with sediment.

Fig. 15 shows the efficiency results for all cases at the end of the flush event (end of the third cycle). It reveals the first obvious conclusion: the flushing event is incapable of fully removing sediment. It also reveals that flushing efficiency strongly depends on the initial sediment height. There is a large variation between 3 and 5 cm. At larger initial heights, the efficiency variation is significantly lower. For larger initial sediment heights, the initial hydraulic conditions (A–F) make little difference in terms of flushing efficiency. Additionally, for these large sediment heights, the final efficiency is close to the initial efficiency, meaning that very little concrete is newly exposed by the flushing event although sediment is transported downstream throughout the tunnel. Flushing efficiency follows a trend such that $A > B > C$ and $D < E < F$. This is expected given that there is more volume and potential energy in Case A than in Case B and in Case B than in Case C (analogous for Cases D, E, and F). Nevertheless, the differences in initial conditions are not very relevant if there is a very thin sediment layer ($h_{sed} \leq 2$). These conditions are relevant for moderate-height layers: $2 \leq h_{sed} \leq 6$. Finally, Fig. 15 shows that opening the gate in 5 or in 10 s has very little impact on the flushing capacity.

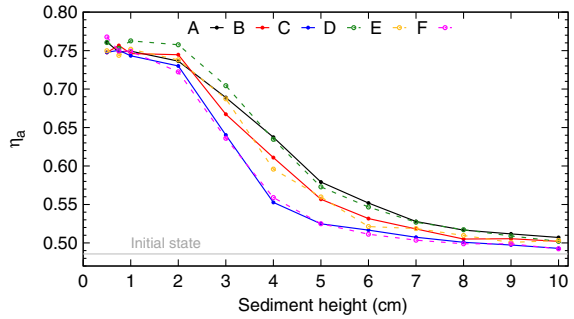

Fig. 15. Flushing efficiency

Overall, the results of the application test show that the numerical model is able to cope with the highly energetic and erosive conditions of real-scale channel flushing. They also show that this type of 2D numerical model is a valuable tool for understanding a range of possible scenarios that allow for better design of hydraulic structures, and for providing insights into better system design and operational guidelines.

In terms of computational effort, the average computational GPU time for a cycle is approximately 240 min, varying between 200 and 400 min. This computational time is very affordable for large-scale sensitivity studies such as the one performed here. An overview of computational time shows this although there is only a slight variation in GPU time in response to the initial sediment depth. Computational GPU time also shows a general trend in which the second flush is on average 20% more costly than the first flush, and that the third flush is on average approximately 14% more costly than the first flush. This is likely due to the fact that there are fewer regions to be cleaned during Flush 3 and so time step reductions are not triggered as often as in other cases.

Conclusions

This paper presents a numerical strategy to deal with finite-depth erodible sediment layers in a shallow-water equations solver and an Exner equation solver. The coupled numerical method is based on a weakly coupled strategy that feeds on a quasi-hyperbolic formulation of the Exner equations. However, similar to positivity-preserving issues in wet/dry fronts computed with the shallow-water equations, the Exner equation may yield negative sediment depths in the presence of a rigid, nonerodible surface under the erodible sediment. A simple but effective strategy is presented and discussed. This strategy relies on analyzing the available sediment mass and the expected sediment fluxes to avoid (during flux computations) possible overerosion in the computational cells. In this way, the more aggressive time-step reduction strategy can be used only as a last resort, when updating sediment mass in the cells, thus minimizing the computational penalty introduced by time-step reduction while ensuring a positivity-preserving sediment evolution.

Two experimental tests show that the strategy performs well under both slow and fast transients. Faster, more energetic, and more violent transients such as dam-break events are of course more challenging for this particular issue. The numerical results compare well with experimental results and indeed show that, given the appropriate bed-load transport law, the numerical model has predictive capabilities in the context of channel cleaning and bed-load transport of finite-depth sediment layers.

A large-scale application was studied, leading to two conclusions: first, that this type of model is applicable to sewer flushing analysis and design; second, that the proposed strategy performs well even under very energetic conditions, with very thin (and therefore potentially troublesome) sediment layers that are quickly swept away by dam-break flows. Furthermore, complex processes of resedimentation and recleaning of particular regions of the computational domain can be solved to ensure sediment-depth-positivity with an acceptable computational effort.

The results in this work show the applicability of 2D depth-averaged models for these types of flows. One-dimensional models have been reported in the literature on the basis that sewer flow is

fundamentally 1D. However, sediment distribution and transport are strongly dependent on the velocity field and on channel geometry. A natural follow-up on applicability is to compare the results of sediment distributions from 1D and 2D models of sewer sediment transport and flushing. Furthermore, in the interest of additional improvement of the predictive capabilities of these types of models, more extensive analysis of transport formulas, including nonequilibrium formulations, is called for.

Acknowledgments

This work was partially funded by the Spanish Ministry of Economy and Competitiveness through Grant MINECO/FEDER CGL2015-66114-R and by the ITN-Programme (Marie Curie Actions) of the European Union's Seventh Framework Programme FP7-PEOPLE-2013-ITN under REA Grant Agreement n_607394-SEDITRANS. The authors would like to acknowledge the collaboration of the Consorcio de Aguas de Bilbao Bizkaia (CABB) for access to the design plans and data for the stormsewer tank tested in this work. The authors also thank the Nvidia Corporation for the hardware donation used in this work through the CUDA Research Center programme.

References

Ashida, K., and Michiue, M. (1972). "Study on the hydraulic resistance and bed-load transport rate in alluvial streams." *Proc. Jpn. Soc. Civil Eng.*, 1972(206), 59–69.

Ashley, R. M., and Verbanck, M. A. (1996). "Mechanics of sewer sediment erosion and transport." *J. Hydraul. Res.*, 34(6), 753–770.

Bakhtyar, R., Barry, D., Jeng, D., and Yeganeh-Bakhtiary, A. (2009). "Modeling sediment transport in the swash zone: A review." *Ocean Eng.*, 227(9–10), 227–240.

Begnudelli, L., and Sanders, F. (2006). "Unstructured grid finite-volume algorithm for shallow-water flow and scalar transport with wetting and drying." *J. Hydr. Eng.*, 10.1061/(ASCE)0733-9429(2006)132:4(371), 371–384.

Bohorquez, P., and Ancey, C. (2015). "Stochastic-deterministic modeling of bed load transport in shallow water flow over erodible slope: Linear stability analysis and numerical simulation." *Earth Surf. Process. Landforms*, 83, 36–54.

Butt, T., and Russel, P. (2000). "Hydrodynamics and cross-shore sediment transport in the swash-zone of natural beaches: A review." *J. Coastal Res.*, 16(2), 255–268.

Campisano, A., Creaco, E., and Modica, C. (2004). "Experimental and numerical analysis of the scouring effects of flushing waves on sediment deposits." *J. Hydrol.*, 299(3–4), 324–334.

Campisano, A., Creaco, E., and Modica, C. (2013). "Numerical modelling of sediment bed aggradation in open rectangular drainage channels." *Urban Water J.*, 10(6), 365–376.

Cao, Z., Day, R., and Egashira, S. (2002). "Coupled and decoupled numerical modeling of flow and morphological evolution in alluvial rivers." *J. Hydr. Eng.*, 10.1061/(ASCE)0733-9429(2002)128:3(306), 306–321.

Castro-Díaz, M., Fernández-Nieto, E., Ferreiro, A., and Parés, C. (2009). "Two-dimensional sediment transport models in shallow water equations. A second order finite volume approach on unstructured meshes." *Comput. Methods Appl. Mech. Eng.*, 198(33–36), 2520–2538.

Creaco, E., and Bertrand-Krajewski, J.-L. (2009). "Numerical simulation of flushing effect on sewer sediments and comparison of four sediment transport formulas." *J. Hydraul. Res.*, 47(2), 195–202.

Dettmar, J. (2007). *A new planning procedure for sewer flushing*, NOVATECH, Lyon, France.

Engelund, F., and Fredsoe, J. (1976). "Sediment transport model for straight alluvial channels." *Nordic Hydrol.*, 7(5), 293–306.

Fernandez-Luque, R., and Beek, R. V. (2010). "Erosion and transport of bed-load sediment." *J. Hydraul. Res.*, 14(2), 127–144.

Fernández-Nieto, E., Lucas, C., de Luna, T. M., and Cordier, S. (2014). "On the influence of the thickness of the sediment moving layer in the definition of the bedload transport formula in Exner systems." *Comput. Fluids*, 91, 87–106.

Furbish, D. J., Haff, P. K., Roseberry, J. C., and Schmeeckle, M. W. (2012). "A probabilistic description of the bed load sediment flux. I: Theory." *J. Geophys. Res.*, 117(F3), 2156–2202.

Grass, A. (1983). "Sediment transport by waves and currents." *Rep. No. Fl29*, SERC, London Center for Marine Technology, London.

Heyman, J., Bohorquez, P., and Ancey, C. (2016). "Entrainment, motion and deposition of coarse particles transported by water over a sloping mobile bed." *J. Geophys. Res.*, 121(10), 1931–1952.

Heyman, J., Ma, H. B., Mettra, F., and Ancey, C. (2014). "Spatial correlations in bed load transport: Evidence, importance and modeling." *J. Geophys. Res.*, 119(8), 1751–1767.

Hou, J., Liang, Q., Zhang, H., and Hinkelmann, R. (2015). "An efficient unstructured MUSCL scheme for solving the 2D shallow water equations." *Environ. Modell. Software*, 66, 131–152.

Hudson, J., and Sweby, P. (2003). "Formulations for numerically approximating hyperbolic systems governing sediment transport." *J. Sci. Comput.*, 19(1–3), 225–252.

Juez, C., Lacasta, A., Murillo, J., and García-Navarro, P. (2016). "An efficient GPU implementation for a faster simulation of unsteady bed-load transport." *J. Hydraul. Res.*, 54(3), 275–288.

Juez, C., Murillo, J., and Garcia-Navarro, P. (2013). "Numerical assessment of bed-load discharge formulations for transient flow in 1D and 2D situations." *J. Hydroinf.*, 15(4), 1234–1257.

Juez, C., Murillo, J., and García-Navarro, P. (2014). "A 2D weakly-coupled and efficient numerical model for transient shallow flow and movable bed." *Adv. Water Resour.*, 71, 93–109.

Kalinske, A. A. (1947). "Movement of sediment as bed load in rivers." *Trans. AGU*, 28(4), 615.

Lacasta, A., Morales-Hernández, M., Murillo, J., and García-Navarro, P. (2014). "An optimized GPU implementation of a 2D free surface simulation model on unstructured meshes." *Adv. Eng. Software*, 78, 1–15.

Leveque, R. (2002). *Finite volume methods for hyperbolic problems*, Cambridge University Press, New York.

Masselink, G., and Russel, P. (2006). "Flow velocities, sediment transport and morphological change in the swash zone of a dissipative and reflective beach." *Mar. Geol.*, 227(3), 227–240.

Meyer-Peter, E., and Müller, R. (1948). "Formulas for bed load transport." *Rep. on Meeting of the Int. Association Hydraulic Structure Research*, Stockholm, Sweden.

Morales de Luna, T., Castro-Díaz, M. J., and Parés Madroñal, M. (2010). "A duality method for sediment transport based on a modified Meyer-Peter & Müller model." *J. Sci. Comput.*, 48(1–3), 258–273.

Morales-Hernández, M., Murillo, J., and García-Navarro, P. (2013). "The formulation of internal boundary conditions in unsteady 2D shallow water flows: Application to flood regulation." *Water Resour. Res.*, 49(1), 471–487.

Murillo, J., and García-Navarro, P. (2010a). "An Exner-based coupled model for two-dimensional transient flow over erodible bed." *J. Comput. Phys.*, 229(23), 8704–8732.

Murillo, J., and García-Navarro, P. (2010b). "Weak solutions for partial differential equations with source terms: Application to the shallow water equations." *J. Comput. Phys.*, 229(11), 4327–4368.

Murillo, J., García-Navarro, P., and Burguete, J. (2009). "Time step restrictions for well-balanced shallow water solutions in non-zero velocity steady states." *Int. J. Numer. Methods Fluids*, 60(12), 1351–1377.

Nielsen, P. (1992). *Coastal bottom boundary layers and sediment transport*, World Scientific, Singapore.

Ortiz, P., Anguita, J., and Riveiro, M. (2015). "Free surface flows over partially erodible beds by a continuous finite element method." *Environ. Earth Sci.*, 74(11), 7357–7370.

Parker, G. (1979). "Hydraulic geometry of active gravel rivers." *J. Hydraul. Div.*, 105(9), 1185–1201.

Rosatti, G., and Zugliani, D. (2015). "Modelling the transition between fixed and mobile bed conditions in two-phase free-surface flows:

The composite Riemann problem and its numerical solution." *J. Comput. Phys.*, 285, 226–250.
Rulot, F., Dewals, B., Erpicum, S., Archambeau, P., and Pirotton, M. (2012). "Modelling sediment transport over partially non-erodible bottoms." *Int. J. Numer. Methods Fluids*, 70(2), 186–199.
Schaffner, J. (2008). "Numerical investigations on the function of flush waves in a reservoir sewer." Ph.D. thesis, Technischen Universität Darmstadt, Darmstadt, Germany.
Schlütter, F. (1999). "Numerical modelling of sediment transport in combined sewer systems." Ph.D. thesis, Aalborg Univ., Aalborg, Denmark.
Shirazi, R. H. S. M., Campisano, A., Modica, C., and Willems, P. (2014). "Modelling the erosive effects of sewer flushing using different sediment transport formulae." *Water Sci. Technol*, 69(6), 1198–1204.
Smart, G. (1984). "Sediment transport formula for steep channels." *J. Hydr. Eng.*, 10.1061/(ASCE)0733-9429(1984)110:3(267), 267–276.
Soares-Frazao, S., and Zech, Y. (2011). "HLLC scheme with novel wave-speed estimators appropiate for two-dimensional shallow-water flow on erodible bed." *Int. J. Numer. Methods Fluids*, 66(8), 1019–1036.
Staufer, P., Dettmar, J., and Pinnekamp, J. (2007). "Impact of the level of approximation on modeling flushing waves." *Water Pract. Technol.*, 2(2), 8.
Struiksma, N. (1999). "Mathematical modelling of bedload transport over non-erodible layers." *Proc., IAHR Symp. on River, Coastal and Estuarine Morphodynamics*, IAHR, Genoa, Italy.
Wu, W. (2004). "Depth-averaged two-dimensional numerical modeling of unsteady flow and nonuniform sediment transport in open channels." *J. Hydr. Eng.*, 10.1061/(ASCE)0733-9429(2004)130:10(1013), 1013–1024.
Xia, J., Lin, B., Falconer, R., and Wang, G. (2010). "Modelling dam-break flows over mobile beds using a 2D coupled approach." *Adv. Water Resour.*, 33(2), 171–183.